molecules

Article

Bodipy Dimer for Enhancing Triplet-Triplet Annihilation Upconversion Performance

Min Gao [1], Le Zeng [2], Linhan Jiang [2], Mingyu Zhang [2], Yong Chen [1,*] and Ling Huang [2,*]

[1] Jiangxi Key Laboratory for Microscale Interdisciplinary Study, Institute for Advanced Study, Nanchang University, Nanchang 330031, China; yaogao@email.ncu.edu.cn
[2] Research Center for Analytical Sciences and Tianjin Key Laboratory of Biosensing and Molecular Recognition, Haihe Laboratory of Sustainable Chemical Transformations, College of Chemistry, Nankai University, Tianjin 300192, China; zengle@dlut.edu.cn (L.Z.); lhjiang@mail.nankai.edu.cn (L.J.); nkuzmy@mail.nankai.edu.cn (M.Z.)
* Correspondence: tychen@ncu.edu.cn (Y.C.); huangl1@nankai.edu.cn (L.H.)

Abstract: Triplet-triplet annihilation upconversion (TTA-UC) has considerable potential for emerging applications in bioimaging, optogenetics, photoredox catalysis, solar energy harvesting, etc. Fluoroboron dipyrrole (Bodipy) dyes are an essential type of annihilator in TTA-UC. However, conventional Bodipy dyes generally have large molar extinction coefficients and small Stokes shifts (<20 nm), subjecting them to severe internal filtration effects at high concentrations, and resulting in low upconversion quantum efficiency of TTA-UC systems using Bodipy dyes as annihilators. In this study, a Bodipy dimer (B-2) with large Stokes shifts was synthesized using the strategy of dimerization of an already reported Bodipy annihilator (B-1). Photophysical characterization and theoretical chemical analysis showed that both B-1 and B-2 can couple with the red light-activated photosensitizer PdTPBP to fulfill TTA-UC; however, the higher fluorescence quantum yield of B-2 resulted in a higher upconversion efficiency (η_{UC}) for PdTPBP/B-2 (10.7%) than for PdTPBP/B-1 (4.0%). This study proposes a new strategy to expand Bodipy Stokes shifts and improve TTA-UC performance, which can facilitate the application of TTA-UC in photonics and biophotonics.

Keywords: triplet-triplet annihilation upconversion; upconversion quantum efficiency; boron-dipyrromethene; Stokes shift; fluorescence quantum yield

Citation: Gao, M.; Zeng, L.; Jiang, L.; Zhang, M.; Chen, Y.; Huang, L. Bodipy Dimer for Enhancing Triplet-Triplet Annihilation Upconversion Performance. *Molecules* **2023**, *28*, 5474. https://doi.org/10.3390/molecules28145474

Academic Editor: Radosław Podsiadły

Received: 20 June 2023
Revised: 10 July 2023
Accepted: 12 July 2023
Published: 18 July 2023

1. Introduction

The photophysical process of photon upconversion converts low-energy photons (long-wavelength light) into high-energy photons (short-wavelength light) [1–5]. Currently, the technology of upconversion luminescence has been extensively utilized in various fields, such as biological imaging [6], 3D printing [7], photocatalysis [8], and solar energy harvesting [9,10]. In particular, triplet-triplet annihilation upconversion (TTA-UC), as the next-generation upconversion material, possesses several distinctive characteristics, such as low excited light power density (~10 mW/cm^2, sunlight illumination), finely tunable excitation and emission wavelengths, and high upconversion quantum efficiency (η_{UC}) [11–13]. TTA-UC generally consists of two components: photosensitizer (Sen) and annihilator (An). As shown in Figure 1a, in a typical TTA-UC process, the Sen absorbs low-energy incident photons and transits to its singlet excited state (^{1}Sen*), and subsequently undergoes an intersystem crossing (ISC) to reach its triplet excited state (^{3}Sen*). Then, the energy is transferred from the ^{3}Sen* to the annihilator (An) through the triplet-triplet energy transfer (TTET) process. Finally, two triplet excited states of annihilators (^{3}An*) collision to operate the triplet-triplet annihilation (TTA) process. One annihilator molecule loses energy and returns to its ground state, while the other annihilator molecule transits to its singlet excited state (^{1}An*) and radiates high-energy upconverted photons [14,15].

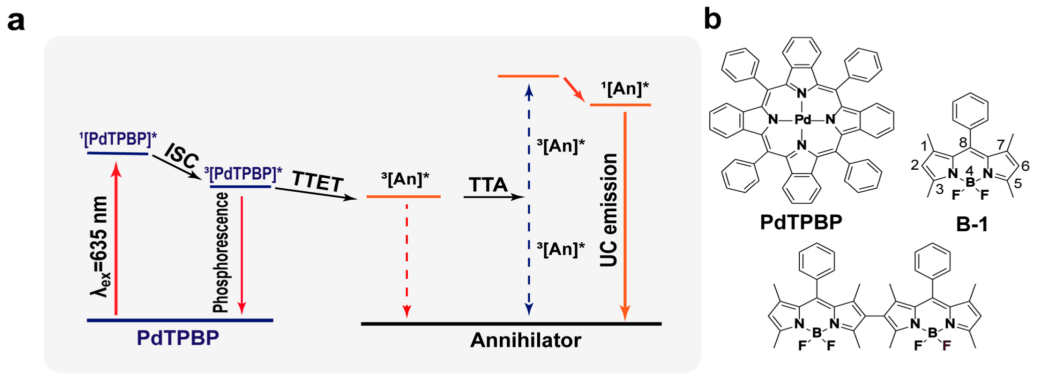

Figure 1. (**a**) Schematic illustration of triplet-triplet annihilation upconversion mechanism; (**b**) Molecular structures of the photosensitizer (PdTPBP) and annihilators (B-1, B-2) in this study.

Developing an efficient TTA-UC system with excellent η_{UC} is essential [16,17], in general, which relies on the manipulation of the physiochemical properties of photosensitizers and annihilators [18]. Various types of photosensitizers with intense absorbance and long-lived triplet states, have been developed in prior investigations to significantly improve η_{UC} [19–22]. In addition, adjusting the triplet state (T_1) of the annihilator can considerably increase the η_{UC} via efficiency improvements in the TTET between the photosensitizer and the annihilator. Pioneering studies have been successful in tuning the T_1 of annihilators for superior η_{UC}, such as diketopyrrolopyrrole (DPP) and tetracene derivatives [23,24]. However, annihilators are often pure organic dyes with no phosphorescence at even low temperatures, making it difficult to determine their T_1 state, so it is difficult to systematically regulate the T_1 energy level of annihilators via a molecular evolution strategy [25]. Boron-dipyrromethene (Bodipy) dyes have been used as model annihilators in TTA-UC because of their high fluorescence quantum yield (Φ_f), robust photostability, and simplicity of chemical functionalization of the molecular structure [26–29]. For instance, it has been confirmed that the pair of PtTPBP and Bodipy could perform red-to-green or red-to-yellow multicolor photon upconversion [30]. Additionally, perylene and Bodipy moieties were incorporated into the dyad annihilator to widen the $\Delta E_{2T1\text{-}S1}$ and greatly boost η_{UC} by driving the TTA process [31]. In addition, the pair of TTA-UC (PtTPBP/Bodipy derivatives) successfully creates a ratio-metric nanothermometer with high thermal sensitivity (7.1% K^{-1}) and resolution (0.1 K) that can precisely monitor temperature changes in vivo. This is facilitated by the steric hindrance of the 1,7-dimethyl substituents of Bodipy, which restricts the free rotation of the phenyl moiety at eight sites in Bodipy [32]. However, the small Stokes shift and large molar extinction coefficient of the Bodipy annihilator cause a serious inner-filter effect, which significantly decrease the Φ_f at high concentrations. Furthermore, modulation of the excited state energy level of Bodipy using the π-extension approach could obtain a negative $\Delta E_{2T1\text{-}S1}$ value, such as in 3,5-distyryl Bodipy [26–29], resulting in a lack of driving force for the TTA process and subsequent decreased upconversion luminescence. The relationship between the T_1 of the Bodipy annihilator and the size of its π-conjugated molecular surface is so poorly understood that it is difficult to regulate their triplet excited states. Therefore, establishing an effective molecular design strategy to regulate the excited states of Bodipy annihilators, specifically the triplet state, remains challenging but intriguing [33,34].

Herein, we describe a dimerization approach at the 2,6-sites of Bodipy to increase the Stokes shift and enhance the performance of the TTA-UC (Figure 1). Compared to the parent Bodipy (B-1), the S_1 of B-2 decreased from 2.43 eV to 2.21 eV, while its T_1 was not reduced significantly after dimerization (1.53 eV vs. 1.52 eV). Calculations based on time-dependent density functional theory (TD-DFT) revealed that the molecular geometry of B-2 tends toward a flat structure in S_1, resulting in a dramatic decrease in S_1 energy level due to an extended π-conjugated surface. In contrast, the two Bodipy moieties tend to have an orthogonal structure in T_1 of B-2, so that the dimerization effect on the T_1 energy level is negligible. Consequently, the double T_1 energy levels of the B-2 are considerably greater than its S_1 ($\Delta E_{2T1\text{-}S1}$ = 0.83 eV), establishing a thermodynamically supported TTA process. Moreover, combining with the red light-absorbing photosensitizer palladium (II) meso-tetraphenyl-tetrabenzoporphyrin (PdTPBP) (Figure 1b), we found that the η_{UC} of B-2/PdTPBP (10.7%) was significantly higher than that of B-1/PdTPBP (4.0%).

2. Results and Discussion

2.1. Characterization of Photophysical Properties of Annihilators

B-2 was synthesized by a palladium-catalyzed cross-coupling reaction (Scheme 1) [35]. The reaction yield increased from 14% to 61% when compared to a previously reported Bodipy dimerization catalyzed by $FeCl_3$ (supporting information). B-2 is soluble in common organic solvents, such as toluene, DCM, and EtOAc. Nuclear magnetic resonance (NMR), as well as mass spectrometry (MS), were used to identify the molecular structure.

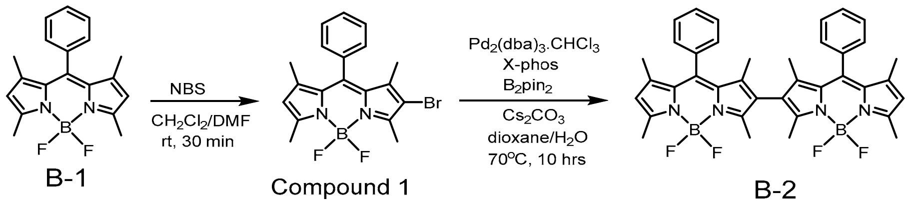

Scheme 1. The preparation process of B-2.

As shown in Figure 2a, compared to that of B-1, the UV–vis absorption spectrum of B-2 was red-shifted from 503 to 536 nm, and the molar extinction coefficient was as high as 1.39×10^5 M^{-1} cm^{-1} (in toluene). The solvent-dependent absorption spectra revealed no change in the absorption profile of B-2, demonstrating that the ground state of B-2 did not undergo charge transfer with the solvent (Figure S1) [36]. The viscosity-dependent absorption spectra of B-1 and B-2 did not exhibit a notable difference (Figure S2).

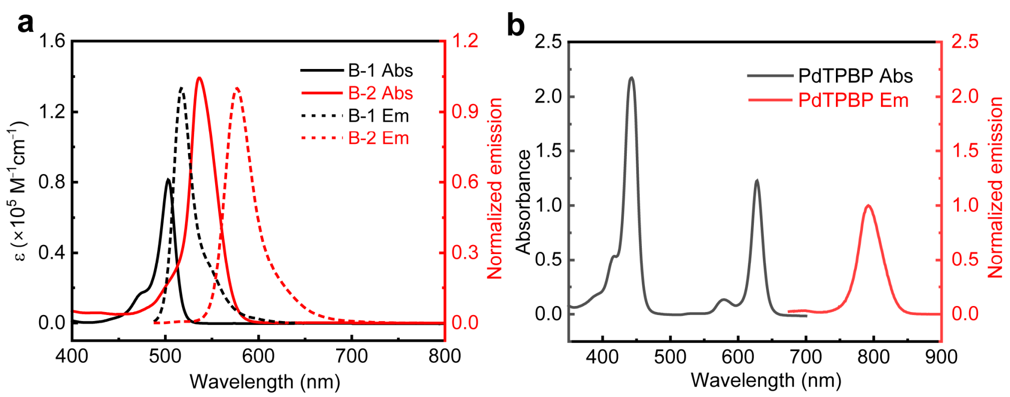

Figure 2. (**a**) UV–vis absorption and fluorescence spectra of B-1 and B-2, λ_{ex} = 470 nm, 10 μM; (**b**) UV–vis absorption and phosphorescence spectra of PdTPBP, λ_{ex} = 635 nm, 10 μM.

The fluorescence emission peak of B-2 is 577 nm, which is longer than that of B-1 at 517 nm (Figure 2a). The intersection of the absorption and fluorescence emission spectra shows that the S_1 of B-1 and B-2 are 2.43 and 2.21 eV, respectively, indicating that the S_1 of Bodipy was effectively reduced after dimerization (Table 1). The absolute Φ_f of B-1 and B-2 at low and high concentrations were then evaluated. The Φ_f of B-1 was 0.72 at a low concentration (10 μM) but 0.42 at a high concentration (1000 μM). However, B-2 retains its Φ_f even at high concentrations (Φ_f = 0.86, 1000 μM) due to its substantial Stokes shift (B-1 vs. B-2, 539 cm^{-1} vs. 1326 cm^{-1}), which suppresses the inner-filter effect at high concentrations. As demonstrated by the polarity-dependent fluorescence emission spectroscopy, the position and width at half maxima of the emission peak of B-1 changed insignificantly, and the fluorescence intensity was not markedly quenched, indicating that intramolecular charge transfer (ICT) and photoinduced electron transfer (PET) had minor effects on the fluorescent properties of B-1 (Figure S3a) [37]. However, the fluorescence emission of B-2 was significantly repressed in acetonitrile, which is presumably due to the low solubility of B-2 in acetonitrile (Figure S3b) [38]. The viscosity-dependent fluorescence spectroscopy of B-2 demonstrated that the fluorescence emission is not viscosity-dependent (Figure S4). To confirm this, we determined the fluorescence lifetime of B-2 at various viscosities (Figure S5). We did not find that the fluorescence lifetime of B-2 got longer as the viscosity went up. This means that the rotation between the two Bodipy moieties or the 8-site phenyl substitutes does not cause excited-state cone crossings, which would quench fluorescence emission [39].

Table 1. The photophysical parameters of B-1 and B-2 in toluene.

Compound	λ_{abs} [a] (nm)	ε [b]	λ_{em} [c] (nm)	Φ_{f1} [d] (%)	Φ_{f2} [e] (%)	τ_f [f] (ns)	S_1 [g] (eV)	$\Delta E_{2T1\text{-}S1}$ [h] (eV)
B-1	503	0.81	517	72	42	3.52	2.43	0.63
B-2	536	1.39	577	92	86	3.25	2.21	0.83

[a] absorption peak; [b] molar extinction coefficient, 10^5 M^{-1} cm^{-1}; [c] fluorescence emission peak; [d] fluorescence quantum yield, 10 μM; [e] fluorescence quantum yield, 1000 μM; [f] fluorescence lifetime; [g] single excited energy level was determined as the crossing point of the absorption and fluorescence emission spectra; [h] thermodynamic driving force for TTA, T_1 state energy level was calculated with TD-DFT.

In addition, we further investigated the redox properties of B-1 and B-2 by cyclic voltammetry versus the Ag/Ag^+ electrode. The oxidation/reduction potentials of B-1 and B-2 were +0.90/−1.59 V and +0.84/−1.51 V, respectively (Figure S6), demonstrating that Bodipy dimerization does not change the redox potential of the annihilator and, thus, does not result in intramolecular charge separation, which causes fluorescence quenching [40].

Next, the triplet-excited state of B-2 was investigated. Due to the high Φ_f and extremely low triplet state quantum yield of B-2, we were unable to directly observe its phosphorescence emission to determine the T_1 energy level. The T_1 of B-2 was approximated using the triplet sensitization bracketing technique. PdTPBP (T_1 = 1.55 eV) and PtTNP (T_1 = 1.36 eV) are two metalloporphyrins with high phosphorescence quantum yield that have been chosen as triplet energy donors. In the presence of 1000 μM B-1 or B-2, we measured the steady and transient photoluminescence spectra of the triplet energy donor. In the presence of B-2, the phosphorescence of PdTPBP at 800 nm decreased by 50.9% (Figure S7), whereas the phosphorescence intensity of PtTNP remained unchanged at 913 nm (Figure S8a). In addition, the phosphorescence intensity of PdTPBP decreased by 33.1% in the presence of B-1, while that of PtTNP was unaffected. The aforementioned experimental results indicate that the T_1 state energy levels of B-1 and B-2 are between 1.36 eV and 1.55 eV.

To gain a deeper understanding of the excited state of B-2, we calculated its properties using time-dependent density functional theory (TD-DFT). Optimization of the ground state (S_0) configuration of B-2 revealed that the dihedral angle between the two Bodipy moieties is 71° (Figure 3a), suggesting that the steric hindrance of the four methyl substituents in B-2 prevents free rotation between the two Bodipy moieties. The scanning of potential energy surface confirms that the energy of B-2 rises rapidly with the increased co-planarization degree between the two Bodipy moieties (Figure S9). The vertical excitation energy of B-2 corresponds well to its UV–vis absorption spectrum (Table S1), showing that the theoretical model used in the DFT-calculations is valid [41]. In contrast to the optimal conformation of the S_0, the S_1 conformation of B-2 discloses that the dihedral angle between the two Bodipy moieties tends to decrease from 71° to 54° (Figure 3a), indicating that the red-shift of the fluorescence emission of B-2 is associated to the extensive π-conjugated surface between the two Bodipy moieties. Furthermore, the significant differences between S_1 and S_0 in the geometrical configuration result in a large Stokes shift of B-2 [42]. Both Bodipy moieties of B-2 have a frontier orbital electron density population, as calculated by the HOMO and LUMO orbitals of B-2 (Figure 3b). This conclusion is attributable to the enhancement of the π-conjugated surface between the Bodipy moieties resulting from the lowering of the dihedral angle, which is directly associated with the prolonged fluorescence emission wavelength of B-2 [43]. The triplet state of B-2 is then investigated using TD-DFT. As shown in Figure 3a, the dihedral angle between the two Bodipy moieties is 69° in the optimized T_1 conformation of B-2, which is no change in the molecular geometry configuration as compared to S_0. Calculation of the triplet state energy levels of B-2 shows that its T_1 and T_2 states are 1.52 eV and 1.53 eV, respectively. The T_1 and T_2 energy levels are close together due to a lack of π-conjugated electron delocalization between the two Bodipy moieties of B-2, resulting in a degenerate T_1 state [42]. The triplet spin density of B-2 is calculated to be populated in both Bodipy moieties, which further confirmed the abovementioned results (Figure 3c) [41]. In this way, B-1 and B-2 exhibit similar T_1 state energy levels (Table S1). The results of the preceding experimental experiments are consistent with the outcomes of the theoretical chemical calculations.

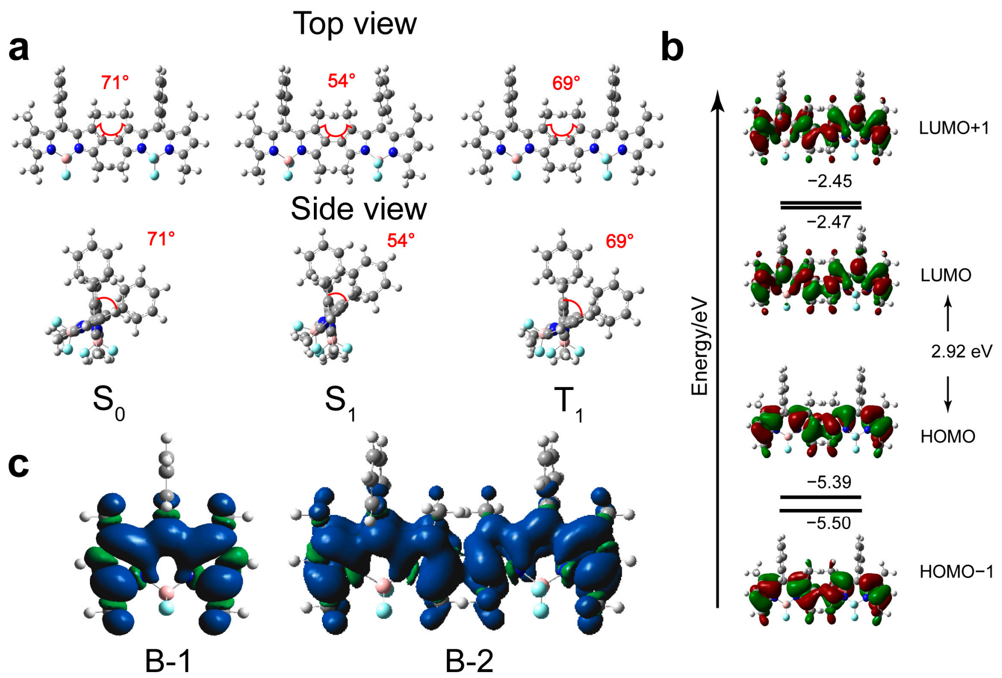

Figure 3. Theoretical chemical calculation results. (**a**) Calculated S_0, S_1, and T_1 configurations of B-2 in toluene, highlighting the dihedral angles between two Bodipy moieties, top panel is the top view, bottom panel is the side view. (**b**) Selected frontier molecular orbitals of B-2 including HOMO, LUMO, HOMO−1, and LUMO+1. (**c**) Triplet state spin density surfaces of B-1 and B-2, respectively, in toluene at the optimized triplet state molecular geometric configurations. Calculated with Gaussian 09 based on the DFT-B3LYP/6-31G.level.

In the case of Bodipy dyes, both S_1 and T_1 decrease as the π-conjugation surface increases, but T_1 decreases more significantly [26–29]. This led to a negative $\Delta E_{2T1\text{-}S1}$ value for most Bodipy derivatives, limiting their utilization in TTA-UC [15]. Despite the fact that a dyad annihilator composed of perylene and Bodipy was developed to address this issue, intramolecular charge transfer causes fluorescence quenching and, as a result, reduced TTA-UC efficiency in highly polar solvents [43]. By regulating the molecular geometric configuration of S_1 and T_1, our proposed Bodipy dimerization strategy raises the Stokes shift of the annihilator to prevent dose-mediated upconversion quenching [24].

2.2. TTA-UC Properties of Annihilators

Following that, we chose the red light-absorbing PdTPBP (T_1 energy level = 1.55 eV [44]) as the photosensitizer to investigate the TTA-UC in relation to B-2. Since PdTPBP has a long triplet state lifetime, its own TTA is not conducive to TTET with the annihilator; thus, a low dose of PdTPBP (10 μM) is used. Because of the close dependence of the TTET and TTA processes on the annihilator concentration, we first optimized the B-2 concentration in TTA-UC (Figure S10) [17]. When the concentration of B-2 exceeded 1000 μM, the TTA-UC intensity stopped increasing and even decreased in the concentration interval 1000–1500 μM. This might be because of the self-absorption and fluorescence quenching with the high dose of B-2 [24]. As a result, we measured the η_{UC} of B-1 and B-2 at 1000 μM, which were determined to be 10.7% and 4.0%, respectively (excited by a 635 nm laser, power intensity = 1267.5 mW/cm^2).

As demonstrated in Figure 4a, the TTA-UC peak of B-2 was redshifted to 600 nm compared to B-1. In particular, the TTA-UC spectrum of B-2 exhibits significantly lower intensity at 630 nm compared to the fluorescence spectrum of B-2. This is due to the strong absorption of PdTPBP at this position (Figure S11), indicating the "emission–reabsorption" effect and that the TTA-UC efficiency of PdTPBP/B-2 should be greater than 10.7%. We further evaluated the color of TTA-UC using Commission Internationale de l'Eclairage (CIE) coordinates (Figure 4b). The CIE coordinates of B-1 and B-2 are (0.35, 0.64) and (0.64, 0.36), respectively, indicating that the molecular structure of the annihilator can be finely tuned to produce multicolor TTA-UC. Simultaneously, we observed the TTA-UC colors of B-1 and B-2 in green and yellow, respectively, with the naked eye under low-power red illumination (Figure 4c). The threshold power intensity (I_{th}) is a critical TTA-UC parameter. The integrated TTA-UC intensity (I_{UC}) has a linear relationship with the incident light power intensity (I_{ex}) when I_{ex} is greater than I_{th} and a nonlinear quadratic relationship when I_{ex} is less than I_{th}. The power-dependent TTA-UC spectra of PdTPBP/B-2 are shown in Figure S12, with a significant increase in I_{UC} with increasing I_{ex}. We found a quadratic relationship between the I_{UC} and the I_{ex} in the low-power intensity region by logarithmic plotting (Figure 4d). This further demonstrates that the B-2 acts as an annihilator to achieve the red-to-yellow TTA-UC. The I_{th} of B-2 (53.7 mW cm^{-2}) is lower than B-1 (76.9 mW cm^{-2}), suggesting that expanding the $\Delta E_{2T1\text{-}S1}$ contributes to the development of TTA-UC pairs with lower I_{th}, which are desirable for solar energy harvesting, photoredox catalysis, and upconversion bioimaging [6]. In addition, the TTA-UC delayed fluorescence lifetime (τ_{DF}) of B-1 and B-2 were measured. The τ_{DF} of B-1 and B-2 were 445.5 μs and 101.4 μs, respectively, which were three orders of magnitude longer than their own τ_f, confirming that this long-lived luminescence was derived from the TTA-UC process [45].

We further measured the TTET efficiency (Φ_{TTET}) of PdTPBP (10 μM) with B-1 (1000 μM) or B-2 (1000 μM) to gain a better understanding of the TTA-UC procedure. The Φ_{TTET} of PdTPBP/B-2 (66.9%) is higher than that of PdTPBP/B-1 (49.1%) (Table 2). In addition, we calculated the triplet state molecular collision cross-section areas of B-1 and B-2 based on DFT theory [46]. The triplet state collision cross-sections of B-1 and B-2 are 1205.0 Bohr^2 and 2206.1 Bohr^2, respectively. The calculation results show that although B-2 has T_1 energy levels similar to B-1, the collision surface of B-2 is greatly extended, which facilitates the Dexter-type triplet energy transfer. Therefore, there is a higher TTET efficiency between PdTPBP and B-2. To further validate our hypothesis, we measured the Stern–Volmer quenching constants (k_{sv}) of B-1 and B-2 for PdTPBP phosphorescence and then calculated their bimolecular quenching constants (k_q). As shown in Table 2, the k_{sv} of B-2 is 9.0 times higher than those of B-1, and the k_q is as high as 2.1×10^7 M^{-1} s^{-1}. The large k_{sv} of B-2 suggests that the dimerization strategy of Bodipy can promote TTET between photosensitizer and annihilator.

Finally, we measured the normalized triplet annihilation efficiencies (η_{TTA}) of B-1 and B-2 using a well-established protocol [47]. The η_{TTA} of PdTPBP/B-1 and PdTPBP/B-2 are 88.0% (39,570 mW/cm^2) and 82.0% (39,570 mW/cm^2), respectively (Figure S13).

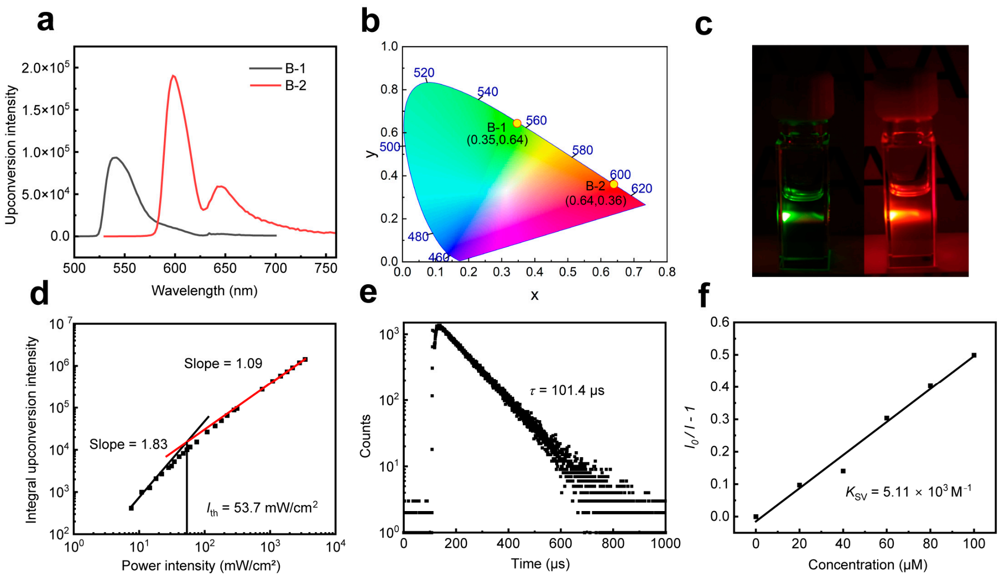

Figure 4. Upconversion properties of the annihilators. (**a**) Upconversion emission spectra of B-1 and B-2 in toluene, λ_{ex} = 635 nm (1267.5 mW/cm^2); (**b**) CIE diagram showing the adjustable upconversion emission colors; (**c**) Upconversion pictures of B-1 and B-2 with PdTPBP; (**d**) Power-dependence of TTA-UC for PdTPBP/B-2, a slope of 1.83 (black, quadratic) and a slope of 1.09 (red, linear), I_{th} is 53.7 mW/cm^2; (**e**) Upconversion lifetime decay trace of PdTPBP/B-2 at 600 nm, in deaerated toluene, PdTPBP (10 µM); (**f**) Stern-Volmer plots of PdTPBP in response to B-2 addition in toluene.

Table 2. The TTA-UC parameters of PdTPBP/B-1 and PdTPBP/B-2 in deaerated toluene.

Compound	η_{UC} [a]	Φ_{TTET} [b] (%)	η_{TTA} [c] (%)	Φ_f [d] (%)	I_{th} [e]	k_{sv} [f]	k_q [g]	τ_{DF} [h] (µs)	T_1 [i] (eV)
B-1	4.0	49.1	88.0	34.3	76.9	0.57	0.23	445.5	1.53
B-2	10.7	66.9	82.0	60.3	53.7	5.11	2.10	101.4	1.52

[a] TTA-UC efficiency at 635 nm CW excitation; [b] triplet-triplet energy transfer efficiency; [c] normalized triplet-triplet annihilation efficiency, 39,570 mW/cm^2; [d] absolute fluorescence quantum yields of annihilators (1000 µM) in the presence of PdTPBP (10 µM); [e] threshold power intensity, mW/cm^2; [f] Stern–Volmer quenching constant, in 10^3 M^{-1}; [g] bimolecular quenching constants, in 10^7 M^{-1} s^{-1}; [h] upconversion fluorescence lifetime. [i] T_1 state energy levels were calculated with TD-DFT.

3. Materials and Methods

3.1. Preparation Process for B-2 [35]

A 25 mL three-necked flask was filled with 2-bromo-Bodipy (compound **1**) (16.2 mg, 0.05 mmol), X-phos (19.0 mg, 40 mol), bis(pinacolato) diboron (B_2pin_2) (5.1 mg, 0.02 mmol), Cs_2CO_3 (65 mg) 1,4-dioxane (5 mL), and H_2O (200 µL). Then, the mixture was degassed with argon for 10 min, followed by the addition of $Pd_2(dba)_3{\cdot}CHCl_3$ (5.2 mg, 5.0 µmol) and another argon degassing for 5 min. After 10 h of reaction at 70 °C, the solvent was evaporated, and the residue was purified using column chromatography on silica with V_{hexane}/V_{DCM} = 1:1 to yield 9.5 mg (yield: 61%). ^{1}H NMR (400 MHz, $CDCl_3$) (ppm): 7.53–7.43 (m, 6H), 7.34–7.22 (m, 4H), 5.99 (s, 2H), 2.56 (s, 6H), 2.35 (s, 6H), 1.37 (s, 6H), 1.12 (s, 6H). ^{13}C NMR (100 MHz, $CDCl_3$) (ppm): 156.06, 154.71, 143.67, 141.74, 141.25, 135.09, 131.80, 131.28, 129.31, 129.18, 129.07, 128.01, 127.89, 124.78, 121.52, 14.70, 14.44, 13.37, 12.90; MS (MALDI) for B-2 ($C_{38}H_{36}B_2F_4N_4$) m/z = 646.31 (calculated), 646.31 (observed).

3.2. Measurement of the Fluorescence Quantum Yields (Φ_f) of B-1 and B-2

The literature has previously reported the fluorescence quantum yields of B-1 and B-2 using the relative method with fluorescein as the reference [48]. We utilized the absolute method based on the integrating sphere to determine the fluorescence quantum yields of B-1 and B-2 with greater precision. The absolute method was used to measure the Φ_f in an FLS1000 photoluminescence spectrometer with an integrating sphere and a xenon lamp as the light source. Φ_f is the total number of emitted photons divided by the total number of absorbed photons. We determined the Φ_f of the annihilators at concentration of 10 μM, 1000 μM as well as the annihilators (1000 μM) in the presence of PdTPBP (10 μM). Since the fluorescence emission spectra of B-2 overlaps with the ultraviolet–visible (UV–vis) absorption spectrum of PdTPBP, the Φ_f of the mixture solution B-2/PdTPBP is lower than that of B-2 alone.

3.3. Measurement of Upconversion Efficiency (η_{UC})

The η_{UC} was calculated with the reference $Ru(bpy)_3Cl_2 \cdot 6H_2O$, which has a photoluminescence quantum yield (Φ_p) of 0.028 in water [49]. The TTA-UC pairs and $Ru(bpy)_3Cl_2 \cdot 6H_2O$ were excited using a 635 nm diode laser (39.8 mW) and a 450 nm diode laser (39.8 mW), respectively. We have uniformed the sensitivity of the fluorometer at different wavelengths. The η_{UC} was calculated using the following equation: eq 1, where η_{UC}, Φ_f, A_{std}, A_{sam}, I_{std}, I_{sam}, η_{std}, and η_{sam} represent the upconversion efficiency, fluorescence quantum yield of reference, reference absorbance (450 nm), PdTPBP absorbance (635 nm), reference integrated photoluminescence intensity, the integral area of the upconversion spectrum, and the refractive index of H_2O (1.333). Note that the theoretical maximum of η_{UC} is standardized to be 1 (100%).

$$\eta_{\mathrm{UC}} = 2 \times \Phi f \times \frac{A_{std}}{A_{sam}} \times \frac{I_{sam}}{I_{std}} \times \left(\frac{\eta_{sam}}{\eta_{std}}\right)^2 \tag{1}$$

3.4. Theoretical Chemical Calculation [50]

All theoretical calculations were performed using the Gaussian 09 program. The ground state geometries of the B-1 and B-2 were optimized using density functional theory (DFT) based on B3LYP/6-31G(d) level. Based on the optimized ground state geometry, the energies of the lowest singlet and triplet excited states were calculated using the TD-DFT method.

4. Conclusions

In conclusion, the new annihilator B-2 was synthesized using the Bodipy dimerization strategy at the 2,6 sites. The η_{UC} was elevated from 4.0% to 10.7% in comparison to the conventional B-1 annihilator. Through theoretical chemical calculations and spectroscopic characterization, it was confirmed that B-2 not only increases the fluorescence quantum yield but also increases the triplet collisional surface to improve the Φ_{TTET}. These above features are extremely important for enhancing the η_{UC}. Thus, this research provides not only a new molecular design strategy for finely regulating the excited state properties of Bodipy-based annihilators but also a new approach for the development of efficient TTA-UC, which will surely promote the use of TTA-UC in photonics and biophotonics fields.

Supplementary Materials: The following supporting information can be downloaded at https://www.mdpi.com/article/10.3390/molecules28145474/s1, Figure S1: absorption spectra of annihilators in different solvents; Figure S2: absorption spectra of annihilators in solutions of different viscosities; Figure S3: Fluorescence spectra of annihilators different solvents; Figure S4: Fluorescence spectra of annihilators with different viscosities; Figure S5: Fluorescence lifetime of annihilators with different viscosities; Figure S6: Cyclic voltammograms of B-1 and B-2; Figure S7: Phosphorescence emission spectra of PdTPBP without annihilators and in the presence of annihilators (determination of TTET efficiency); Figure S8: Phosphorescence emission spectra and phosphorescence lifetime of PtTNP without annihilators and in the presence of annihilators; Figure S9: Ground state potential energy curves of B-2, as a function of the dihedral angle between two moieties B-2 (step: 10°); Figure S10: (a) The upconversion emission spectra of PdTPBP (10 μM) and different concentrations of B-1 in degassed toluene, (b) quantitative analysis of the relationship between upconversion intensity and concentration of B-1. λex = 635 nm, (c) The upconversion emission spectra of PdTPBP (10 μM) and different concentrations of B-2 in degassed toluene, (d) quantitative analysis of the relationship between upconversion intensity and concentration of B-2. λex = 635 nm; Figure S11: Fluorescence spectra of B-2 (1 mM) with or without photosensitizer; Figure S12: (a) Incident light power dependence study of TTA-upconversion analysis; Figure S13: ηTTA determination of annihilator compounds; Figure S14: The excitation spectrum of B-2 in toluene, λem = 600 nm; Figure S15: 1H-NMR (400 MHz, $CDCl_3$) of B-1; Figure S16; ^{1}H-NMR (400 MHz, $CDCl_3$) of B-2; Figure S17: ^{13}C-NMR (100 MHz, $CDCl_3$) of B-2; Figure S18: HRMS (MALDI) of B-2; Table S1: Density functional theory (DFT) calculation for the annihilators. Table S2: S1 and T1 energy levels of B-1, B-2, obtained by experiments, CAM-B3LYP, and B3LYP calculations. The reference [51–57] is in the Supplementary Material.

Author Contributions: B-1 and B-2 were produced and purified by M.G., who also tested their steady-state spectra and upconversion luminescence. L.J. and M.Z. performed transient spectroscopy; L.Z. handled the data analysis, while Y.C. and L.H. wrote the original draft of the study and revised it. All authors have read and agreed to the published version of the manuscript.

Funding: Research start-up fund of Nankai University, Tianjin Natural Science Foundation (No. S22QNG922), National Natural Science Fund for Excellent Young Scientists Fund Program (Overseas) (No. 013398), and the Open Fund of the State Key Laboratory of Fine Chemicals (Dalian University of Technology) (No. KF2111).

Institutional Review Board Statement: Not applicable.

Informed Consent Statement: Not applicable.

Data Availability Statement: The data reported are contained within the manuscript and Supplementary Materials.

Conflicts of Interest: The authors declare no conflict of interest.

Sample Availability: Not applicable.

References

1. Zhou, B.; Shi, B.; Jin, D.; Liu, X. Controlling upconversion nanocrystals for emerging applications. *Nat. Nanotechnol.* **2015**, *10*, 924–936. [CrossRef]
2. Wen, S.; Zhou, J.; Schuck, P.J.; Suh, Y.D.; Schmidt, T.W.; Jin, D. Future and challenges for hybrid upconversion nanosystems. *Nat. Photonics* **2019**, *13*, 828–838. [CrossRef]
3. Liu, X.; Yan, C.H.; Capobianco, J.A. Photon upconversion nanomaterials. *Chem. Soc. Rev.* **2015**, *44*, 1299–1301. [CrossRef]
4. Dong, H.; Sun, L.D.; Yan, C.H. Energy transfer in lanthanide upconversion studies for extended optical applications. *Chem. Soc. Rev.* **2015**, *44*, 1608–1634. [CrossRef]
5. Dong, H.; Du, S.R.; Zheng, X.Y.; Lyu, G.M.; Sun, L.D.; Li, L.D.; Zhang, P.Z.; Zhang, C.; Yan, C.H. Lanthanide Nanoparticles: From Design toward Bioimaging and Therapy. *Chem. Rev.* **2015**, *115*, 10725–10815. [CrossRef]
6. Huang, L.; Kakadiaris, E.; Vaneckova, T.; Huang, K.; Vaculovicova, M.; Han, G. Designing next generation of photon upconversion: Recent advances in organic triplet-triplet annihilation upconversion nanoparticles. *Biomaterials* **2019**, *201*, 77–86. [CrossRef]
7. Sanders, S.N.; Schloemer, T.H.; Gangishetty, M.K.; Anderson, D.; Seitz, M.; Gallegos, A.O.; Stokes, R.C.; Congreve, D.N. Triplet fusion upconversion nanocapsules for volumetric 3D printing. *Nature* **2022**, *604*, 474–478. [CrossRef]
8. Ravetz, B.D.; Pun, A.B.; Churchill, E.M.; Congreve, D.N.; Rovis, T.; Campos, L.M. Photoredox catalysis using infrared light via triplet fusion upconversion. *Nature* **2019**, *565*, 343–346. [CrossRef]
9. Gholizadeh, E.M.; Prasad, S.K.K.; Teh, Z.L.; Ishwara, T.; Norman, S.; Petty, A.J., II; Cole, J.H.; Cheong, S.; Tilley, R.D.; Anthony, J.E.; et al. Photochemical upconversion of near-infrared light from below the silicon bandgap. *Nat. Photonics* **2020**, *14*, 585–590. [CrossRef]
10. Richards, B.S.; Hudry, D.; Busko, D.; Turshatov, A.; Howard, I.A. Photon Upconversion for Photovoltaics and Photocatalysis: A Critical Review. *Chem. Rev.* **2021**, *121*, 9165–9195. [CrossRef]
11. Singh-Rachford, T.N.; Castellano, F.N. Photon upconversion based on sensitized triplet–triplet annihilation. *Coord. Chem. Rev.* **2010**, *254*, 2560–2573. [CrossRef]
12. Gao, C.; Wong, W.W.H.; Qin, Z.; Lo, S.C.; Namdas, E.B.; Dong, H.; Hu, W. Application of Triplet-Triplet Annihilation Upconversion in Organic Optoelectronic Devices: Advances and Perspectives. *Adv. Mater.* **2021**, *33*, e2100704. [CrossRef]
13. Yanai, N.; Kimizuka, N. Stimuli-Responsive Molecular Photon Upconversion. *Angew. Chem. Int. Ed.* **2020**, *59*, 10252–10264. [CrossRef]
14. Zhou, J.; Liu, Q.; Feng, W.; Sun, Y.; Li, F. Upconversion luminescent materials: Advances and applications. *Chem. Rev.* **2015**, *115*, 395–465. [CrossRef]
15. Zeng, L.; Huang, L.; Han, J.; Han, G. Enhancing Triplet-Triplet Annihilation Upconversion: From Molecular Design to Present Applications. *Acc. Chem. Res.* **2022**, *55*, 2604–2615. [CrossRef]

16. Ji, S.; Wu, W.; Wu, W.; Guo, H.; Zhao, J. Ruthenium(II) polyimine complexes with a long-lived 3IL excited state or a 3MLCT/3 IL equilibrium: Efficient triplet sensitizers for low-power upconversion. *Angew. Chem. Int. Ed.* **2011**, *50*, 1626–1629. [CrossRef]
17. Huang, L.; Wu, W.; Li, Y.; Huang, K.; Zeng, L.; Lin, W.; Han, G. Highly Effective Near-Infrared Activating Triplet-Triplet Annihilation Upconversion for Photoredox Catalysis. *J. Am. Chem. Soc.* **2020**, *142*, 18460–18470. [CrossRef]
18. Harada, N.; Sasaki, Y.; Hosoyamada, M.; Kimizuka, N.; Yanai, N. Discovery of Key TIPS-Naphthalene for Efficient Visible-to-UV Photon Upconversion under Sunlight and Room Light. *Angew. Chem. Int. Ed.* **2021**, *60*, 142–147. [CrossRef]
19. Zhao, J.; Ji, S.; Guo, H. Triplet–triplet annihilation based upconversion: From triplet sensitizers and triplet acceptors to upconversion quantum yields. *RSC Adv.* **2011**, *1*, 937–950. [CrossRef]
20. Zhao, J.; Xu, K.; Yang, W.; Wang, Z.; Zhong, F. The triplet excited state of Bodipy: Formation, modulation and application. *Chem. Soc. Rev.* **2015**, *44*, 8904–8939. [CrossRef]
21. Pristash, S.R.; Corp, K.L.; Rabe, E.J.; Schlenker, C.W. Heavy-Atom-Free Red-to-Yellow Photon Upconversion in a Thiosquaraine Composite. *ACS Appl. Energy Mater.* **2019**, *3*, 19–28. [CrossRef]
22. Borisov, S.M.; Saf, R.; Fischer, R.; Klimant, I. Synthesis and properties of new phosphorescent red light-excitable platinum(II) and palladium(II) complexes with Schiff bases for oxygen sensing and triplet-triplet annihilation-based upconversion. *Inorg. Chem.* **2013**, *52*, 1206–1216. [CrossRef]
23. Pun, A.B.; Campos, L.M.; Congreve, D.N. Tunable Emission from Triplet Fusion Upconversion in Diketopyrrolopyrroles. *J. Am. Chem. Soc.* **2019**, *141*, 3777–3781. [CrossRef]
24. Fallon, K.J.; Churchill, E.M.; Sanders, S.N.; Shee, J.; Weber, J.L.; Meir, R.; Jockusch, S.; Reichman, D.R.; Sfeir, M.Y.; Congreve, D.N.; et al. Molecular Engineering of Chromophores to Enable Triplet-Triplet Annihilation Upconversion. *J. Am. Chem. Soc.* **2020**, *142*, 19917–19925. [CrossRef]
25. Filatov, M.A. Heavy-atom-free BODIPY photosensitizers with intersystem crossing mediated by intramolecular photoinduced electron transfer. *Org. Biomol. Chem.* **2019**, *18*, 10–27. [CrossRef]
26. Loudet, A.; Burgess, K. BODIPY Dyes and Their Derivatives: Syntheses and Spectroscopic Properties. *Chem. Rev.* **2007**, *107*, 4891–4932. [CrossRef]
27. Lu, H.; Mack, J.; Yang, Y.; Shen, Z. Structural modification strategies for the rational design of red/NIR region BODIPYs. *Chem. Soc. Rev.* **2014**, *43*, 4778–4823. [CrossRef]
28. Kowada, T.; Maeda, H.; Kikuchi, K. BODIPY-based probes for the fluorescence imaging of biomolecules in living cells. *Chem. Soc. Rev.* **2015**, *44*, 4953–4972. [CrossRef]
29. Ziessel, R.; Harriman, A. Artificial light-harvesting antennae: Electronic energy transfer by way of molecular funnels. *Chem. Commun.* **2011**, *47*, 611–631. [CrossRef]
30. Singh-Rachford, T.N.; Haefele, A.; Ziessel, R.; Castellano, F.N. Boron Dipyrromethene Chromophores: Next Generation Triplet Acceptors/Annihilators for Low Power Upconversion Schemes. *J. Am. Chem. Soc.* **2008**, *130*, 16164–16165. [CrossRef]
31. Turshatov, A.; Busko, D.; Avlasevich, Y.; Miteva, T.; Landfester, K.; Baluschev, S. Synergetic effect in triplet-triplet annihilation upconversion: Highly efficient multi-chromophore emitter. *Chemphyschem* **2012**, *13*, 3112–3115. [CrossRef]
32. Xu, M.; Zou, X.; Su, Q.; Yuan, W.; Cao, C.; Wang, Q.; Zhu, X.; Feng, W.; Li, F. Ratiometric nanothermometer in vivo based on triplet sensitized upconversion. *Nat. Commun.* **2018**, *9*, 2698. [CrossRef]
33. Sun, W.; Ronchi, A.; Zhao, T.; Han, J.; Monguzzi, A.; Duan, P. Highly efficient photon upconversion based on triplet–triplet annihilation from bichromophoric annihilators. *J. Mater. Chem. C* **2021**, *9*, 14201–14208. [CrossRef]
34. Yang, M.; Sheykhi, S.; Zhang, Y.; Milsmann, C.; Castellano, F.N. Low power threshold photochemical upconversion using a zirconium(iv) LMCT photosensitizer. *Chem. Sci.* **2021**, *12*, 9069–9077. [CrossRef]
35. Hayashi, Y.; Yamaguchi, S.; Cha, W.Y.; Kim, D.; Shinokubo, H. Synthesis of Directly Connected BODIPY Oligomers through Suzuki–Miyaura Coupling. *Org. Lett.* **2011**, *13*, 2992–2995. [CrossRef]
36. Zanini, G.P.; Montejano, H.A.; Previtali, C.M. Specific solvent effects on the charge separation efficiency in photoinduced electron transfer processes. *J. Photoch. Photobio. A* **2000**, *132*, 161–166. [CrossRef]
37. Zhang, B.; Wang, S.; Tan, J.; Zhang, X. Unique fluorescence of boronic acid derived salicylidenehydrazone complexes with two perpendicular ICT: Solvent effect on PET process. *Dyes Pigm.* **2018**, *155*, 186–193. [CrossRef]
38. Zhu, S.; Zhang, J.; Vegesna, G.; Luo, F.-T.; Green, S.A.; Liu, H. Highly Water-Soluble Neutral BODIPY Dyes with Controllable Fluorescence Quantum Yields. *Org. Lett.* **2011**, *13*, 438–441. [CrossRef]
39. Liu, X.; Chi, W.; Qiao, Q.; Kokate, S.V.; Cabrera, E.P.; Xu, Z.; Liu, X.; Chang, Y.T. Molecular Mechanism of Viscosity Sensitivity in BODIPY Rotors and Application to Motion-Based Fluorescent Sensors. *ACS Sens.* **2020**, *5*, 731–739. [CrossRef]
40. Purc, A.; Espinoza, E.M.; Nazir, R.; Romero, J.J.; Skonieczny, K.; Jezewski, A.; Larsen, J.M.; Gryko, D.T.; Vullev, V.I. Gating That Suppresses Charge Recombination-The Role of Mono-N-Arylated Diketopyrrolopyrrole. *J. Am. Chem. Soc.* **2016**, *138*, 12826–12832. [CrossRef]
41. Mattiello, S.; Mecca, S.; Ronchi, A.; Calascibetta, A.; Mattioli, G.; Pallini, F.; Meinardi, F.; Beverina, L.; Monguzzi, A. Diffusion-Free Intramolecular Triplet–Triplet Annihilation in Engineered Conjugated Chromophores for Sensitized Photon Upconversion. *ACS Energy Lett.* **2022**, *7*, 2435–2442. [CrossRef]
42. Chen, Y.; Zhao, J.; Guo, H.; Xie, L. Geometry relaxation-induced large Stokes shift in red-emitting borondipyrromethenes (BODIPY) and applications in fluorescent thiol probes. *J. Org. Chem.* **2012**, *77*, 2192–2206. [CrossRef]

43. Cui, X.; Zhao, J.; Lou, Z.; Li, S.; Wu, H.; Han, K.L. Switching of the triplet excited state of rhodamine/naphthaleneimide dyads: An experimental and theoretical study. *J. Org. Chem.* **2015**, *80*, 568–581. [CrossRef]
44. Huang, L.; Le, T.; Huang, K.; Han, G. Enzymatic enhancing of triplet-triplet annihilation upconversion by breaking oxygen quenching for background-free biological sensing. *Nat. Commun.* **2021**, *12*, 1898. [CrossRef]
45. Suresh, S.M.; Duda, E.; Hall, D.; Yao, Z.; Bagnich, S.; Slawin, A.M.Z.; Bassler, H.; Beljonne, D.; Buck, M.; Olivier, Y.; et al. A Deep Blue B,N-Doped Heptacene Emitter That Shows Both Thermally Activated Delayed Fluorescence and Delayed Fluorescence by Triplet-Triplet Annihilation. *J. Am. Chem. Soc.* **2020**, *142*, 6588–6599. [CrossRef]
46. Wünderlich, D.; Scarlett, L.H.; Briefi, S.; Fantz, U.; Zammit, M.C.; Fursa, D.V.; Bray, I. Application of molecular convergent close-coupling cross sections in a collisional radiative model for the triplet system of molecular hydrogen. *J. Phys. D Appl. Phys.* **2021**, *54*, 115201. [CrossRef]
47. Olesund, A.; Johnsson, J.; Edhborg, F.; Ghasemi, S.; Moth-Poulsen, K.; Albinsson, B. Approaching the Spin-Statistical Limit in Visible-to-Ultraviolet Photon Upconversion. *J. Am. Chem. Soc.* **2022**, *144*, 3706–3716. [CrossRef]
48. Zhang, X.-F. BisBODIPY as PCT-based halogen free photosensitizers for highly efficient excited triplet state and singlet oxygen formation: Tuning the efficiency by different linking positions. *Dyes Pigm.* **2017**, *146*, 491–501. [CrossRef]
49. Shokri, S.; Wiederrecht, G.P.; Gosztola, D.J.; Ayitou, A.J.-L. Photon Upconversion Using Baird-Type (Anti)Aromatic Quinoidal Naphthalene Derivative as a Sensitizer. *J. Phys. Chem. C* **2017**, *121*, 23377–23382. [CrossRef]
50. Frisch, M.J.; Trucks, G.W.; Schlegel, H.B.; Scuseria, G.E.; Robb, M.A.; Cheeseman, J.R.; Scalmani, G.; Barone, V.; Mennucci, B.; Petersson, G.A.; et al. *Gaussian 09, Revision D.01*; Gaussian, Inc.: Wallingford, CT, USA, 2013.
51. Mu, Y.-d.; Guo, D.-c.; Hou, Y.-j.; Wang, S.-h. Facile electrospinning preparation and superior luminescence properties of BODIPY composite nanofibers. *Text. Res. J.* **2016**, *87*, 1795–1805. [CrossRef]
52. Nepomnyashchii, A.B.; Broring, M.; Ahrens, J.; Bard, A.J. Synthesis, photophysical, electrochemical, and electrogenerated chemiluminescence studies. Multiple sequential electron transfers in BODIPY monomers, dimers, trimers, and polymer. *J. Am. Chem. Soc.* **2011**, *133*, 8633–8645. [CrossRef]
53. Singh, V.K.; Yu, C.; Badgujar, S.; Kim, Y.; Kwon, Y.; Kim, D.; Lee, J.; Akhter, T.; Thangavel, G.; Park, L.S.; et al. Highly efficient organic photocatalysts discovered via a computer-aided-design strategy for visible-light-driven atom transfer radical polymerization. *Nat. Catal.* **2018**, *1*, 794–804. [CrossRef]
54. Deng, F.; Sun, W.; Castellano, F.N. Texaphyrin sensitized near-IR-to-visible photon upconversion. *Photochem. Photobiol. Sci.* **2014**, *13*, 813–819. [CrossRef]
55. Mattiello, S.; Monguzzi, A.; Pedrini, J.; Sassi, M.; Villa, C.; Torrente, Y.; Marotta, R.; Meinardi, F.; Beverina, L. Self-Assembled Dual Dye-Doped Nanosized Micelles for High-Contrast Up-Conversion Bioimaging. *Adv. Funct. Mater.* **2016**, *26*, 8447–8454. [CrossRef]
56. Kwon, T.-H.; Kim, M.K.; Kwon, J.; Shin, D.-Y.; Park, S.J.; Lee, C.-Y.; Kim, J.-J.; Hong, J.-I. Highly Efficient Light-Harvesting System Based on a Phosphorescent Acceptor Coupled with Dendrimer Donors via Singlet-Singlet and Triplet-Triplet Energy Transfer. *Chem. Mater.* **2007**, *19*, 3673–3680. [CrossRef]
57. Li, J.K.; Zhang, M.Y.; Zeng, L.; Huang, L.; Wang, X.Y. NIR-Absorbing B,N-Heteroarene as Photosensitizer for High-Performance NIR-to-Blue Triplet-Triplet Annihilation Upconversion. *Angew. Chem. Int. Ed.* **2023**, *62*, e202303093. [CrossRef]